El Niño and the shifting geography of cholera in Africa

Sean M. Moore[a,b,c], Andrew S. Azman[a], Benjamin F. Zaitchik[d], Eric D. Mintz[e], Joan Brunkard[e], Dominique Legros[f], Alexandra Hill[f], Heather McKay[a], Francisco J. Luquero[g,h], David Olson[h], and Justin Lessler[a,1]

[a]Department of Epidemiology, Johns Hopkins Bloomberg School of Public Health, Baltimore, MD 21205; [b]Department of Biological Sciences, University of Notre Dame, Notre Dame, IN 46556; [c]Eck Institute for Global Health, University of Notre Dame, Notre Dame, IN 46556; [d]Department of Earth and Planetary Sciences, Johns Hopkins University, Baltimore, MD 21218; [e]Division of Foodborne, Waterborne and Environmental Diseases, Centers for Disease Control and Prevention, Atlanta, GA 30329; [f]Department of Pandemic and Epidemic Diseases, World Health Organization, 1211, Geneva, Switzerland; [g]Epicentre, 75012 Paris, France; [h]Department of International Health, Johns Hopkins Bloomberg School of Public Health, Baltimore, MD 21205; and [i]Médecins Sans Frontières, 75011 Paris, France

Edited by Andrea Rinaldo, Laboratory of Ecohydrology (ECHO/IIE/ENAC), Ecole Polytechnique Federale Lausanne, and approved March 8, 2017 (received for review October 18, 2016)

The El Niño Southern Oscillation (ENSO) and other climate patterns can have profound impacts on the occurrence of infectious diseases ranging from dengue to cholera. In Africa, El Niño conditions are associated with increased rainfall in East Africa and decreased rainfall in southern Africa, West Africa, and parts of the Sahel. Because of the key role of water supplies in cholera transmission, a relationship between El Niño events and cholera incidence is highly plausible, and previous research has shown a link between ENSO patterns and cholera in Bangladesh. However, there is little systematic evidence for this link in Africa. Using high-resolution mapping techniques, we find that the annual geographic distribution of cholera in Africa from 2000 to 2014 changes dramatically, with the burden shifting to continental East Africa—and away from Madagascar and portions of southern, Central, and West Africa—where almost 50,000 additional cases occur during El Niño years. Cholera incidence during El Niño years was higher in regions of East Africa with increased rainfall, but incidence was also higher in some areas with decreased rainfall, suggesting a complex relationship between rainfall and cholera incidence. Here, we show clear evidence for a shift in the distribution of cholera incidence throughout Africa in El Niño years, likely mediated by El Niño's impact on local climatic factors. Knowledge of this relationship between cholera and climate patterns coupled with ENSO forecasting could be used to notify countries in Africa when they are likely to see a major shift in their cholera risk.

cholera | El Niño Southern Oscillation | disease mapping | climate and health | Bayesian mapping

Improvements to water and sanitation have eliminated the threat of cholera throughout much of the world; however, each year, millions are infected and over a hundred thousand die in Asia, Africa, and the Caribbean (1). Cholera's impact may be the greatest in Africa, where there has been ongoing circulation since the 1970s (2) and unexpected, explosive epidemics have been associated with case fatality rates (CFRs) as high as 50% (commonly 1–15%) (3, 4). Reported CFRs for Africa remain twice as high as the 2014 global average of 1.2% (5). Cholera epidemics in sub-Saharan Africa have proven difficult to forecast, hampering prevention and control efforts (6, 7). However, it has long been believed that climatic factors in general, and the El Niño Southern Oscillation (ENSO) in particular, are important drivers of cholera incidence (8, 9).

ENSO is a periodic, multiannual variation in sea surface temperatures and winds in the tropical Pacific Ocean that influences weather patterns globally (10, 11). Warm phases in the eastern Pacific Ocean (El Niño events) occur every 2–7 y and are associated with warm sea surface temperatures in parts of the western Indian Ocean, above-average rainfall in East Africa, and below-average rainfall in dry regions of southern Africa and the Sahel (Fig. 1*A*). The 2015–2016 El Niño event is only the third of the past 40 y to be classified as "strong" or "very-strong" (joining 1982–1983 and 1997–1998; Fig. 1*D*) (12). The global link between cholera and climate has been the subject of inquiry since at least the 19th century (13). Most modern research has focused on South Asia, where interannual variability in seasonal cholera epidemic size has been associated with ENSO strength (8, 14, 15).

Warm sea surface temperatures in the Bay of Bengal that often accompany El Niño events may facilitate the growth of environmental reservoirs of *Vibrio cholerae*, increasing the severity of that year's epidemic (8, 14, 16). In sub-Saharan Africa, however, the majority of cholera cases occur in inland regions (17), hence sea surface temperatures are unlikely to play as direct a role in driving seasonal and multiannual variations in cholera incidence. There is some evidence that cholera incidence in the Great Lakes Region of East Africa increases during abnormally warm El Niño events (18, 19). Large cholera epidemics in Africa are also associated with both very dry and very wet conditions: dry conditions may force people to use unsafe drinking water sources (17, 20, 21), whereas flooding may facilitate fecal contamination of drinking water (22). This complexity combined with the lack of fine-scale data on cholera incidence and environmental covariates has limited our understanding of how climatic events, like El Niño, impact cholera incidence on the continent.

Whereas vulnerability to cholera outbreaks is driven by local conditions, including safe water and sanitation access, health infrastructure, and socioeconomic factors, ENSO-related climate perturbations may also modify the distribution of cholera risk. To understand how ENSO affects the geographic distribution of cholera incidence in Africa, we mapped estimated cholera incidence at the scale of 20 × 20 km grid cells throughout the continent. Using a hierarchical Bayesian approach, we

Significance

In the wake of the 2015–2016 El Niño, multiple cholera epidemics occurred in East Africa, including the largest outbreak since the 1997–1998 El Niño in Tanzania, suggesting a link between El Niño and cholera in Africa. However, little evidence exists for this link. Using high-resolution mapping techniques, we found the cholera burden shifts to East Africa during and following El Niño events. Throughout Africa, cholera incidence increased three-fold in El Niño-sensitive regions, and 177 million people experienced an increase in cholera incidence. Without treatment, the case fatality rate can reach 50%, but accessible, appropriate care nearly eliminates mortality. Climatic forecasts predicting El Niño events 6–12 mo in advance could trigger public health preparations and save lives.

Author contributions: S.M.M., A.S.A., B.F.Z., E.D.M., F.J.L., and J.L. designed research; S.M.M., A.S.A., B.F.Z., E.D.M., F.J.L. and J.L. conceived this study; S.M.M., A.S.A., B.F.Z., J.B., D.L., A.H., H.M., F.J.L., D.O., and J.L. performed research; S.M.M., A.S.A., B.F.Z., D.L., A.H., H.M., F.J.L., D.O., and J.L. contributed to the collection, assembly, and entry of data; S.M.M., A.S.A., B.F.Z., and J.L. analyzed data; and S.M.M., A.S.A., and J.L. wrote the paper.

The authors declare no conflict of interest.

This article is a PNAS Direct Submission.

Freely available online through the PNAS open access option.

[1]To whom correspondence should be addressed. Email: justin@jhu.edu.

This article contains supporting information online at www.pnas.org/lookup/suppl/doi:10.1073/pnas.1617218114/-/DCSupplemental.

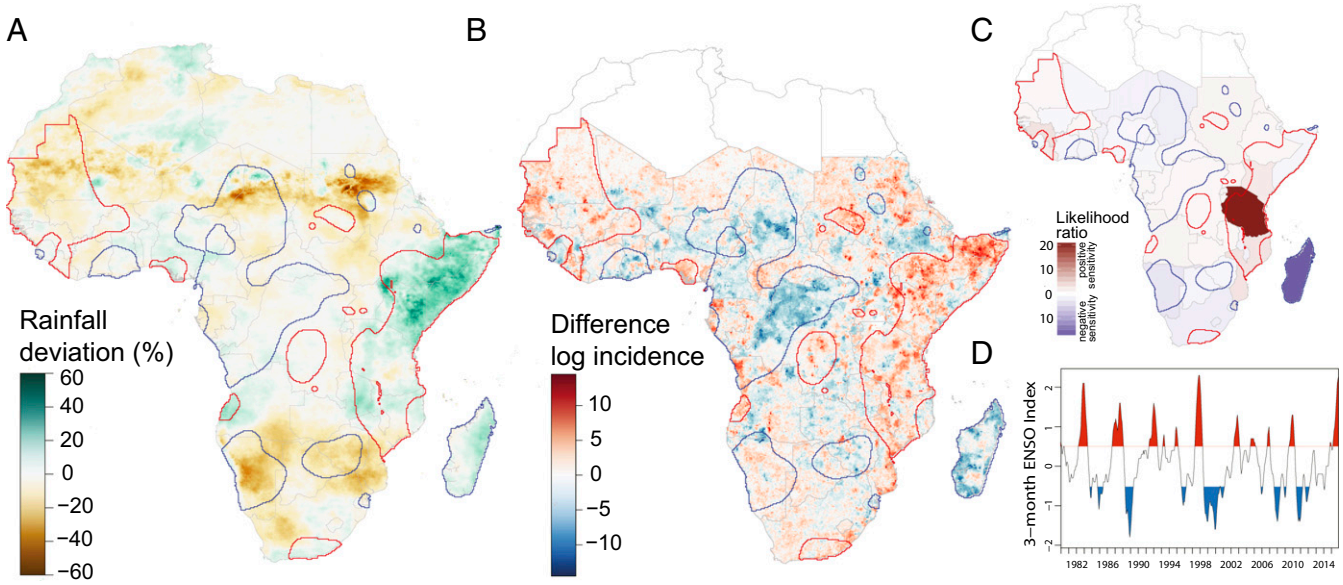

Fig. 1. Geographical distribution of cholera in El Niño and non-El Niño years. (*A*) Rainfall anomalies in El Niño years, 1980–2015. (*B*) Fine-scale geographic distribution of cholera anomalies in El Niño years, 2000–2014. (*C*) Country-level cholera anomalies in El Niño years, based on WHO reports, 1980–2015. The colors represent the likelihood ratio in support of a significant difference in cholera incidence between El Niño and non-El Niño years. (*D*) History of strength of ENSO anomalies, 1980–2015. El Niño years are in red, and La Niña years are in blue. Red and blue outlines in *A*–*C* represent regions with positive (red) and negative (blue) sensitivity to El Niño events in cholera incidence selected by smoothing the normalized difference in cholera incidence using a kernel smoothing algorithm with a bandwidth of 150 km and then clustering areas into areas where cholera incidence is positively sensitive, negatively sensitive, and insensitive to El Niño events (Fig. 2).

integrated data from over 17,000 annual observations of cholera incidence from 2000 to 2014 in over 3,000 unique locations of varying spatial extent, ranging from entire countries to neighborhoods. The resulting maps reflect modeled cholera incidence at a fine spatial resolution using reported counts of cholera cases, key explanatory variables (population density, access to improved drinking water, access to improved sanitation, and distance to nearest major water body), and a spatially dependent covariance term (*Materials and Methods*). We then examined the potential mechanistic association between ENSO-related changes in cholera incidence and several environmental variables including rainfall.

Results

El Niño events affect the distribution and magnitude of cholera incidence throughout the African continent (Figs. 1*B* and 2). Africa as a whole experienced a similar number of cholera cases in El Niño years compared with non-El Niño years between 2000–2014 [215,546 (95% credible interval [CrI]: 209,770–221,704) vs. 209,791 (95% CrI: 202,087–219,047)], but the geographic distribution of these cases fundamentally changed between El Niño and non-El Niño years, with most countries experiencing areas of both decreased and increased incidence (Fig. 1*B*). However, notable regional patterns were observed; southern Africa experienced fewer cholera cases in El Niño years (31,598 fewer cases; 95% CrI: 29,385–33,775), whereas continental East Africa (i.e., excluding Madagascar) had significant increases in cholera incidence in El Niño years (Fig. 1*B*), with 48,670 (95% CrI: 45,192–52,053) excess cases (*SI Appendix*, Table S4). Overall, 177 million people live in areas where annual cholera incidence increased by at least 1 per 100,000 during El Niño years (95% CrI: 166.0–189.5 million), and 81 million live in areas where annual incidence increased by more than 1 per 10,000 (95% CrI: 75.8–86.4 million). Likewise, 137 million live in areas where annual incidence declined by at least 1 per 100,000 (95% CrI: 125.6–149.4 million) and 69 million live in areas where annual incidence decreased by more than 1 per 10,000 (95% CrI: 63.2–74.2 million).

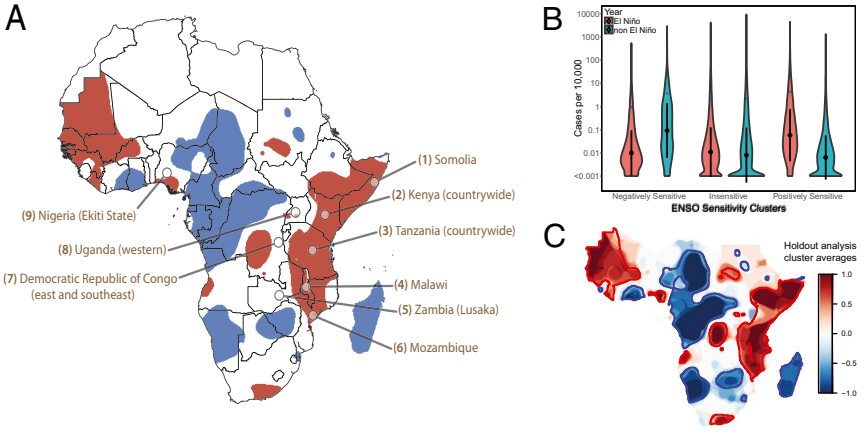

Fig. 2. Geographical distribution and incidence rates for El Niño-sensitive regions. (*A*) Regions with positive (red) and negative (blue) sensitivity to El Niño events in cholera incidence. Areas selected by smoothing the normalized difference in cholera incidence using a kernel smoothing algorithm with a bandwidth of 150 km, then clustering areas into areas where cholera incidence is positively sensitive (red), negatively sensitive (blue) and insensitive (white) to El Niño events. Callouts indicate major reported outbreaks of the 2015–16 cholera season (*SI Appendix, 1. SI Materials and Methods*). (*B*) Kernel density (violin) plot of cases per 10,000 in different El Niño-sensitive regions during El Niño and non-El Niño years. Black circles are grid cell-level medians ± 1 SD and blue diamonds are grid-cell level means. (*C*) Overlay of El Niño sensitive clusters from holding out each El Niño or non-El Niño pair of years with negatively sensitive clusters = −1 (blue) and positively sensitive clusters = 1 (red).

To delineate areas that can expect significant increases or reductions in cholera incidence during El Niño years, we classified areas, irrespective of political boundaries, based on the sensitivity of local cholera incidence to El Niño using clustering and smoothing algorithms. We identified those areas with the largest increase in expected incidence during El Niño events (the top quartile) and those with the largest decrease (the bottom quartile, see *Materials and Methods*). The largest positively sensitive cholera cluster extends through continental East Africa from the horn of Africa down to Mozambique, with smaller clusters scattered throughout the continent (Fig. 2*A*). The most distinct negatively sensitive clusters are in Madagascar and portions of Central and West Africa (Fig. 2*A*). Overall, 45.8% of people in sub-Saharan Africa live in El Niño-sensitive areas: 263.6 million in positively sensitive clusters and 203.7 million in negatively sensitive ones. During El Niño years, cholera incidence within positively sensitive clusters increased, on average, almost threefold from 1.1 per 10,000 to 3.3 per 10,000 [relative rate (RR): 2.91; 95% CrI: 2.52–3.19], corresponding to almost 55,000 excess cases (Fig. 2*B*). In negatively sensitive clusters incidence decreased from 4.2 per 10,000 to 2.2 per 10,000 (RR: 0.53, 95% CrI: 0.48–0.57), a reduction of nearly 40,000 cases. A sensitivity analysis showed that the locations of these clusters were not driven by a single year or El Niño event, (Fig. 2*C*).

Because we were only able to perform fine-scale mapping of cholera incidence from 2000 to 2014, there are a limited number of El Niño events captured in these analyses (2 weak, 2 moderate, and 0 strong/very-strong events; *SI Appendix*, Table S2). To confirm that recently observed geographic patterns hold over a longer time scale, we analyzed country-level incidence data reported to the WHO dating back to 1980 (23). Similar to the fine-scale analyses, increases in cholera incidence are concentrated in continental East Africa, specifically Tanzania and Kenya, where El Niño events are associated with increased rainfall and generally wet conditions (Fig. 1*A*), whereas the largest decreases are in Madagascar and Namibia. There is a significant positive association between ENSO strength and cholera incidence in continental East Africa with above-average rainfall during El Niño events (Fig. 1 *A* and *C*), with incidence increasing by 29,226 (95% CrI: 9,403–49,049) cases for every unit increase in the annual peak ENSO index value (*SI Appendix*, Fig. S45 and *2. SI Further Results*).

At the continental scale there was no strong association between rainfall patterns and cholera incidence. However, areas of higher cholera incidence during El Niño years were concentrated in river basins where rainfall anomalies were either below average (RR: 4.4 in basins with rainfall anomalies in the lowest quartile; $P < 0.001$; 95% CrI: 2.5–7.8) or above average (RR: 2.4 in basin with rainfall anomalies in the upper quartile; $P = 0.003$; 95% CrI: 1.4–4.2) compared with areas where rainfall anomalies were insignificant (Fig. 3). In addition, higher cholera incidence during El Niño years was also concentrated in river basins with an above-average normalized difference vegetation index (NDVI), evapotranspiration, and temperature (*SI Appendix*, Figs. S22–S26). The positive association between higher rainfall and higher cholera incidence was concentrated in continental East and southern Africa (encompassing much of the positively sensitive regions in Fig. 1*A*), although this association was only significant in continental East Africa (RR: 3.5; 95% CrI: 1.4–9.0; Fig. 3*C*). Cholera incidence in West and Central Africa showed no clear positive association with rainfall, but incidence was significantly higher in areas of East Africa (RR: 4.7; 95% CrI: 1.6–13.5), West Africa (RR: 6.8; 95% CrI: 2.3–20.3), and Central Africa (RR: 18.7; 95% CrI: 3.7–94.4) with below-average rainfall during El Niño years (Fig. 3*C*).

Positive El Niño-associated rainfall anomalies were concentrated in positively sensitive cholera clusters. This association was due to positive rainfall anomalies in continental East Africa, as rainfall during El Niño years was either normal or below average in the positively sensitive cholera clusters in the other geographic regions (*SI Appendix*, Fig. S28). The local association between cholera incidence and rainfall anomalies was not constant across the continent and varied by mean annual rainfall levels. In drier areas, cholera incidence increased during both low and high rainfall years, whereas in the wettest areas, cholera incidence tends to be below average during high rainfall years (*SI Appendix*, Fig. S27). The concentration of high-rainfall areas in West and Central Africa may explain the lack of correlation between increased rainfall and cholera incidence in these regions, whereas the large region of low to moderate rainfall in East Africa may be responsible for the positive relationship between increased rainfall and cholera incidence observed during El Niño events. Cholera incidence in coastal areas is positively associated with sea surface temperature anomalies, particularly where anomalies are >0.2 °C; however, these regions also have positive rainfall anomalies (*SI Appendix*, *2. SI Further Results*).

Discussion

The annual reported incidence of cholera in sub-Saharan Africa did not differ significantly between El Niño and non-El Niño years from 2000 to 2014. However, we found evidence of a large-scale shift in incidence within the continent, highlighted by a large increase in cholera incidence in East Africa during and after El Niño events resulting in almost 50,000 additional annual cases. In addition to this large positively sensitive region, we identified several other regions with increased cholera incidence during El Niño events, as well as several regions in Central and West Africa that appear to be negatively sensitive to El Niño events, with decreased incidence during these years. Although we did not find a strong, continent-wide association between El Niño-associated meteorological anomalies and changes in cholera incidence, increased incidence was associated with positive rainfall anomalies in eastern and southern Africa, suggesting that these relationships may vary from place to place and should be assessed at a small scale.

The 2015–2016 surge in cholera cases in East Africa was not used in these analyses to define cholera clusters, but, nevertheless, these outbreaks are concentrated in positively El Niño-sensitive areas (Fig. 2*A*). Since August 2015, Tanzania has experienced a nation-wide outbreak that has infected 25,482 and killed 299 as of May 17, 2016. Somalia, Kenya, Malawi, Uganda, and Mozambique have also experienced outbreaks since the summer of 2015 (*SI Appendix*, *1. SI Materials and Methods*). These outbreaks (including Tanzania but excluding Somalia; *SI Appendix*, *1. SI Materials and Methods*) have resulted in at least 34,800 reported cases since August 2015, a finding that does not include the peak 2016 cholera season in most of these countries. This result equates to nearly 25,000 more cases than would be expected over the same time period during non-El Niño years, and in-line with the 34,713 cases (95% CrI: 31,043–38,018) estimated from our analyses for these countries during a moderate El Niño year. At the edge of the East African positively sensitive cluster, eastern Democratic Republic of Congo has been experiencing high cholera incidence, although this trend started before the current El Niño event. Cholera has not, however, been confined to positively sensitive clusters. El Niño-insensitive regions of western Uganda have recently experienced several small outbreaks, as has the Ekiti state of Nigeria and Lusaka, Zambia.

The presented shifts in cholera burden associated with El Niño events are based on estimates of reported incidence, not true incidence, due to a lack of specific information regarding spatial and temporal reporting biases. Although evidence suggests there are country-specific reporting biases for cholera that lead to both overestimation of cholera incidence during some epidemics and the underestimation of true cholera incidence in other settings (24), as long as these biases are not temporally variable they should not influence the association of cholera with ENSO. However, if the size of outbreaks are systematically underreported, then the magnitude of the shift in cholera incidence during El Niño events may be underestimated due to missed cases. Case over- or underestimation would not shift the direction of El Niño-sensitivity unless the quality of surveillance and reporting efforts were associated with the occurrence of El

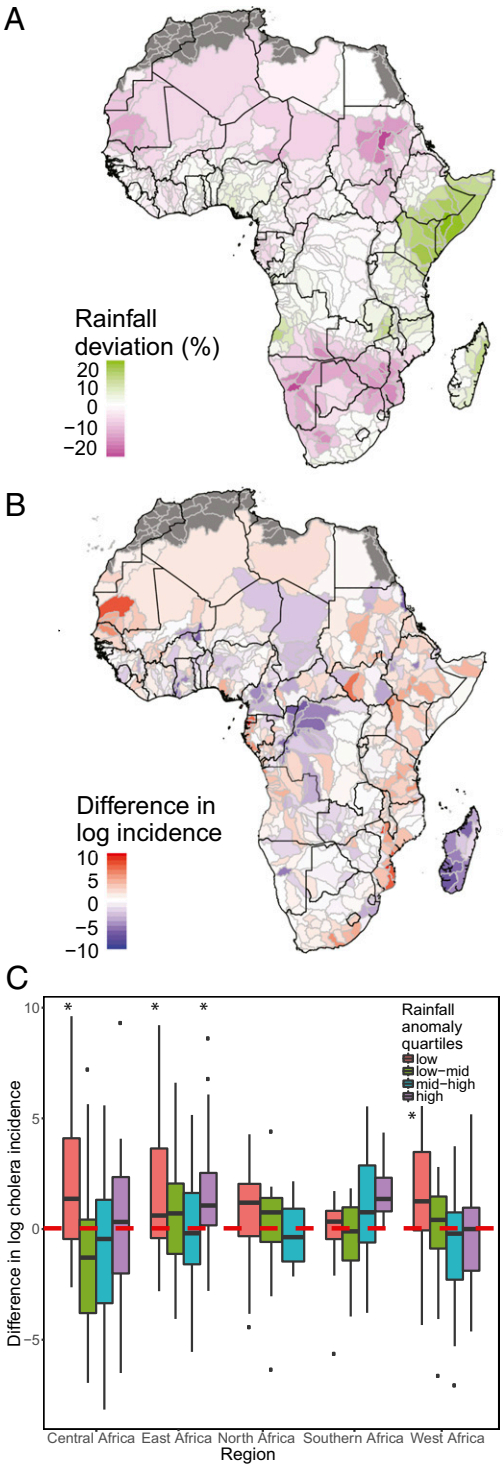

Fig. 3. Association between cholera and rainfall by river basin. (*A* and *B*) River basin-level rainfall anomalies (anomalies smaller than ±5% not shown) (*A*) and (log) cholera anomalies (*B*) between El Niño and non-El Niño years. (*C*) River basin-level cholera incidence anomalies by region and the strength of rainfall anomalies. Positive cholera anomalies are associated with negative rainfall anomalies (lowest quartile) in every region and positive rainfall anomalies (highest quartile) in East and Southern Africa. *The difference in log cholera incidence between El Niño and non-El Niño years for a given rainfall anomaly quartile and geographical region is significantly different from the difference in log incidence for areas within that region with rainfall anomalies that fall in the low to mid or mid to high ranges (second and third quartiles).

Niño events. We have not found any evidence of increased or decreased surveillance due to ENSO patterns. However, regions where cholera cases are underreported or not reported at all may be incorrectly categorized as ENSO-insensitive due to a lack of information about when cholera cases occur in these areas.

Several recent studies have found that extreme El Niño events could become more frequent due to climate change (25–27). This finding suggests that shifts in cholera associated with El Niño events may become more pronounced in the future, perhaps shifting the cholera burden toward East Africa. The behavior of ENSO under climate change and its future impacts on Africa are, however, active topics of research, so projections are highly uncertain (28). Moreover, ENSO is only one way in which greenhouse gas induced warming influences the African climate. In the Horn of Africa, for example, El Niño is associated with wet conditions and higher rates of cholera (Fig. 1). However, the Horn of Africa has experienced significant drying in recent decades (29). Furthermore, although the majority of global climate models project that the region will get wetter in the 21st century, these models have systematic errors in representing the seasonal distribution of Horn of Africa rainfall and could be producing spurious projections (30). Thus, it is not clear how a potential increase in wet El Niño extremes superimposed on a warming-induced drying trend in the Horn of Africa would affect overall cholera risk in that region.

Predicting local cholera incidence is a difficult task. However, here we show clear evidence for a shift in the distribution of cholera incidence throughout regions of Africa in El Niño compared with non-El Niño years, likely mediated by El Niño's impact on local climatic factors. Recent ENSO forecasting models warn of developing El Niño conditions up to 12 mo in advance (31). As predictive ability of ENSO anomalies improves (31, 32), our findings provide hope that we may be able to provide early cholera-risk forecasts. Because effective case management dramatically decreases mortality in cholera outbreaks, and new control tools (e.g., oral cholera vaccines) may prevent, or at least limit, outbreaks, the ability to step up surveillance, preparedness and response when local risk is high can have a significant impact on saving lives. A better understanding of the mechanisms by which El Niño changes the distribution of cholera incidence will help us elucidate the effect of climatic change on the global distribution of cholera risk.

Materials and Methods

Cholera Data. The cholera data used to generate the fine-scale maps of cholera incidence were collated from 360 separate datasets (details and data are available at www.iddynamics.jhsph.edu/projects/cholera-dynamics/data). Annual case counts reported to the WHO from 2000 to 2014 were included for each country in sub-Saharan Africa (23). Further details on data sources are provided in *SI Appendix, 1. SI Materials and Methods*. The datasets included in our analysis included cholera case counts aggregated at various time scales from daily to yearly. To estimate annual incidence rates, observations at subannual time scales were aggregated to the annual level, although many aggregated annual observations cover only part of a calendar year. A total of 17,033 annual observations from 3,071 unique locations from 2000 to 2014 were included in the main analysis (Dataset S1). These 3,071 unique locations include 44 different countries, 327 first-level administrative units, 1,948 second-level administrative units, and 752 locations at the third-level administrative unit or lower (*SI Appendix*, Fig. S1). A summary of the cholera data used to model the spatial distribution of cholera incidence is provided by country (*SI Appendix*, Tables S1 and S2 and *1. SI Materials and Methods*).

Although our database does not cover 2015 and 2016, we used three primary sources for data to provide an overview of the main cholera epidemics that have occurred since the onset of the 2015–2016 El Niño event, assumed to be April 1, 2015 (*SI Appendix*, Table S3). First, we performed a query on HealthMap.org (March 21, 2016) for the disease cholera using all sources and restricted to Africa. Second, we obtained updated situation reports from the WHO for all available countries. Finally, we used the weekly data reported from UNICEF's West Africa regional office as of week 6, 2016 (33).

Covariates and Climate Variables. Gridded population density at a 1km^2 resolution for the entire African continent were obtained from WorldPop (www.worldpop.org.uk; accessed March 30, 2016). Distance to the coast was calculated from a shapefile of the African coastline using the "rgeos" package in R (34). Distances to the nearest large lake or reservoir (surface area: >50 km^2) and to the nearest permanent smaller water bodies including rivers (surface area: >0.1 km^2) were calculated using the level one and level two layers from the Global Lakes and Wetlands Database (35). The proportion of the population with access to improved drinking water (*SI Appendix*, Fig. S2), improved sanitation (*SI Appendix*, Fig. S3), and open defecation were obtained from ref. 36. All covariate data were resampled to the same 20 km resolution using the "raster" package in R (37).

Gridded rainfall at a spatial resolution of 0.05° from 1981 through 2015 was obtained from Climate Hazards Group InfraRed Precipitation with Station data version 2.0 (38). Rainfall totals were aggregated at an annual time scale running according to the El Niño cycle, which runs from July to June rather than the calendar year. Gridded mean temperature, soil moisture, and evapotranspiration data at a 0.25° spatial resolution were obtained from the Global Land Data Assimilation System (39). Annual NDVI values at 0.05° from 2000 to 2014 were aggregated from monthly MODIS data (40). Monthly sea surface temperatures at a 2.0° spatial resolution from 2000 to 2014 were obtained from the Extended Reconstructed Sea Surface Temperature dataset (41). For each climate variable long-term annual means were calculated for the periods from 2000 to 2014 and 1981 to 2014 (rainfall only), and deviations from these long-term means were calculated for El Niño years. All land-based climate variables were resampled to 20 × 20 km using the raster package in R (37).

El Niño Analyses. We classified each year as having no El Niño anomaly, or as being a weak, moderate or strong El Niño year based on the Oceanic Niño Index (ONI) used by the National Oceanic and Atmospheric Administration. Monthly ONI values are calculated from the 3-mo running mean of sea surface temperatures anomalies in the Niño 3.4 region of the Pacific Ocean (5°N–5°S, 120°W–170°W). A year with at least 5 consecutive months with an ONI value ≥0.5 °C is classified as an El Niño event; and El Niño events with at least 3 consecutive months ≥1.0 °C, 1.5 °C, or 2.0 °C are classified as moderate, strong, or very strong events, respectively (Fig. 1*D*). El Niño events typically overlap calendar years, so we classified El Niño years as running from July through June of the following calendar year. Because the majority of the available cholera data are aggregated at an annual level we classified cholera cases occurring during both calendar years overlapping an El Niño event as associated with an El Niño year. For example, the very strong 1997–1998 El Niño event translates to an 1997 El Niño year and cholera cases from both 1997 and 1998 were considered to be associated with the 1997–1998 event.

Using ONI values, from 2000 to 2014, the years 2000, 2001, 2008, 2011, 2012, 2013, and 2014 were classified as non-El Niño years. The years from 2004 to 2007 were classified as weak El Niño events with ONI values of ≥0.5 °C but <1 °C, and 2002–2003 and 2009–2010 were classified as moderate-to-strong El Niño years with ONI values ≥1 °C for a minimum of 3 mo. The analysis presented in the main text included both weak and moderate-to-strong El Niño events as El Niño years. In *SI Appendix, 2.3 Sensitivity to the Definition of El Niño Years*, we present an analysis using only moderate-to-strong El Niño years to understand how the main results vary with different El Niño classifications.

Mapping Methodology. A hierarchical Bayesian modeling framework was used to map aggregated cholera observational data to underlying incidence rates. The entire study region was divided into N_j = 73,979 20 × 20 km grid cells, with any grid cells entirely covered by water or with a population density of 0 excluded from analysis. The annual cholera incidence in each grid cell, λ_j, was modeled using a log-linear regression equation,

$$\log(\lambda_j) = \beta_0 + \beta_p X_{p,j} + \psi_j,$$

with covariates $X_{p,j}$. The random effects, ψ_j, account for any overdispersion and spatial correlation in the data and are modeled by a conditional autoregressive distribution (42, 43). Spatial correlation between random effects is determined by a binary N_j *X* N_j adjacency matrix, *A*, with element $a_{j,k}$ equal to one if grid cells (j, k) are neighbors (sharing an edge), and zero otherwise (and for $j = k$). The joint distribution of ψ is an N_j-dimensional multivariate normal distribution given by

$$\psi_j \sim N\left(0, \sigma_v^2 (D - \rho A)^{-1}\right),$$

where ρ is a parameter representing the relative strength of spatial dependence with $0 \le \rho < 1$ and *D* is a diagonal matrix with entries $d_{j,j} = \sum_{k=1}^{N_j} a_{j,k}$, where $d_{j,j}$ represents the number of neighbors for grid cell *j* (44–46).

Each observation, Y_i, was mapped to the underlying grid cells that are within area *i* and were modeled by a Poisson process:

$$Y_i \sim Pois(E_i).$$

The expected number of cases, E_i, for each observation is the sum of the expected number of cases in each grid cell:

$$E_i = \sum_{j=1}^{N_i} \lambda_j * p_j,$$

where p_j is the size of the population in grid cell *j*. Each area-based observation was associated with a polygon and the determination of which grid cells were associated with each observation was performed by using the 'extract' function from the raster library in R (37). For point-based observations, such as geolocated case data or cases from a single refugee camp, the grid cell containing that GPS point was used. Multiple observations for the same area covering different temporal periods or from different sources were treated as independent observations, and data from different, but overlapping, spatial scales were also treated as independent observations.

The intercept term of the log-linear regression model, β_0 and the regression parameters $\beta = (\beta_1, \ldots, \beta_p)$ were assigned weakly informative Gaussian prior distributions, $N(0,10)$. The spatial autocorrelation parameter ρ was assigned a β (2,1) prior and the precision parameter τ_v from the spatial autocorrelation term ψ_j was assigned a $\Gamma(0.5,0.0005)$ prior distribution. The covariates included in our analysis were level of access to improved drinking water, level of access to improved sanitation, population density, distance to the nearest coastline, and distance to the nearest major waterbody. The relationship between cholera incidence and these covariates was considered separately for El Niño and non-El Niño years to determine whether their relationship was altered by weather patterns associated with the ENSO cycle. Details on model implementation are provided in *SI Appendix*, and summary model outputs are provided in Datasets S2–S5.

To test the sensitivity of our results to single El Niño or La Niña events, we reran the model while holding out each single pair of years representing either an El Niño event or a non-El Niño event (eight pairs of years; with the exception of the non-El Niño year 2008, between the 2006–2007 and 2009–2010 El Niño events, where only a single year was withheld from the analysis). The variation in incidence when different El Niño and non-El Niño years were withheld are presented in *SI Appendix*, Figs. S14 and S15. The sensitivity of the shift in incidence during El Niño events to holding out different years is presented in *SI Appendix*, Fig. S16.

Clustering of Cholera El Niño-Sensitive Regions. El Niño-sensitive regions were identified by smoothing maps of normalized cholera incidence and then clustering the smoothed incidence by quartiles. Cholera incidence was first normalized by dividing the difference in cholera incidence in El Niño versus non-El Niño years by the square root of the summed variance from El Niño and non-El Niño years. The distribution function of the normalized cholera incidence was then smoothed using a kernel smoother with a bandwidth of 150 km and grid cells weighted by population density (47, 48). Smoothing was implemented using the image.smooth function in the "fields" R package (49). The results of the smoothing and subsequent clustering with alternative bandwidth sizes ranging from 50 to 300 km are shown in *SI Appendix*, Fig. S17. Grid cells in the lowest quartile were classified as negatively sensitive clusters, whereas grid cells in the upper quartile were classified as positively sensitive clusters. Grid cells in the middle quartiles were classified as insensitive. The sensitivity of the clustering results to holding out each pairing of El Niño and non-El Niño years is presented in Fig. 2*C*.

Country-Level ENSO Anomalies. In addition to using the detailed incidence estimates data from 2000 to 2014, we also used official country-level annual reports from the WHO dating back to 1980 to understand the relationship between El Niño years and cholera incidence (23). The results presented in Fig. 1*C* are based on a linear regression models for each country of the form:

$$\sqrt{C_y} = \beta_0 + \beta_1 \mathbb{I}(y \in EN) + E_y,$$

where, C_y is the number of cases in year *y* and *EN* represents the set of years with an El Niño event. We explored variants of this model that included a linear term for trends in reporting over time and those using *EN* sets (i.e., weak and stronger or moderate and stronger). Within Fig. 1*C*, we

highlighted countries based on the likelihood ratio comparing models with and without β_1, with the darker colors illustrating larger support for a significant different between El Niño and non-El Niño years.

Association of Cholera with Local Climate. We examined the spatial distribution of the following six climatic factors estimated from remote sensing and climate reanalysis in El Niño and non-El Niño years between 2000 and 2014: rainfall, temperature, NDVI, soil moisture, evapotranspiration, and sea surface temperature. Of the five land-based factors, deviations in rainfall differed by >20% over the largest proportion of the sub-Saharan African land area (5.0%; Fig. 3*A*). Because of its strong association with El Niño events, high correlation with other climatic factors, and clear mechanistic relationship with cholera transmission, here we focus primarily on the relationship between rainfall and cholera (analyses of other climatic factors are included in *SI Appendix, 2. SI Further Results*). The association between rainfall and cholera was examined by aggregating ENSO-associated rainfall anomalies and incidence at the river-basin scale because of the impact of rainfall within a river basin on local surface water and flooding. The major river basins of Africa, along with their subbasins used in this analysis, were obtained from the World Wildlife Fund HydroSHEDS project (50). Because we did not observe a simple linear relationship between ENSO-associated shifts in climate and cholera at the continental- or basin-scale, the relationship between climate measures and shifts in cholera incidence at the basin-scale were tested by aggregating climate anomalies into quartiles and then comparing shifts in cholera incidence in the areas with climate anomalies in the lower and upper quartiles to areas not experiencing significant anomalies (middle quartiles) using one-way ANOVA tests. These statistical tests allow us to determine whether large ENSO-associated negative or positive shifts in climate variables such as rainfall are associated with shifts in cholera incidence.

ACKNOWLEDGMENTS. We thank Abdinasar Abubakar for providing information about current cholera outbreaks; Carla Zelaya, Marisa Hast, Kerry Shannon, Susan Fallon, Chris Troeger, and Yuru Huang for assistance with identifying, extracting, and entering data; and the Johns Hopkins Infectious Disease Dynamics group for feedback on study design and analysis. Research by S.M.M., A.S.A., H.M., and J.L. was supported by Bill and Melinda Gates Foundation Grant OPP1127318. B.F.Z. was supported by National Science Foundation Grant 1639214 ["Innovations at the Nexus of Food, Energy, and Water Systems (Track 1): Understanding multi-scale resilience options for vulnerable regions"]. Cholera data were provided by the Ministries of Health of Benin, Democratic Republic of Congo, Mozambique, South Sudan, and Nigeria. Additional cholera data were provided by Médecins Sans Frontières (MSF) and MSF/Epicentre, the WHO, and the United Nations Relief Agency. Data are indexed at www.iddynamics.jhsph.edu/projects/cholera-dynamics/data and are either directly available or available by request of the owning agency.

1. World Health Organization (2015) Cholera, 2014. *Wkly Epidemiol Rec* 90:517–528.
2. Mutreja A, et al. (2011) Evidence for several waves of global transmission in the seventh cholera pandemic. *Nature* 477:462–465.
3. Siddique AK, et al. (1995) Why treatment centres failed to prevent cholera deaths among Rwandan refugees in Goma, Zaire. *Lancet* 345:359–361.
4. Mengel MA, Delrieu I, Heyerdahl L, Gessner BD (2014) Cholera outbreaks in Africa. *Curr Top Microbiol Immunol* 379:117–144.
5. WHO (2015) Cholera case fatality rate: Situations and trends. Available at www.who.int/gho/epidemic_diseases/cholera/case_fatality_rate_text/en. Accessed May 5, 2016.
6. Constantin de Magny G, Guégan J-F, Petit M, Cazelles B (2007) Regional-scale climate-variability synchrony of cholera epidemics in West Africa. *BMC Infect Dis* 7:20.
7. Reyburn R, et al. (2011) Climate variability and the outbreaks of cholera in Zanzibar, East Africa: A time series analysis. *Am J Trop Med Hyg* 84:862–869.
8. Pascual M, Rodó X, Ellner SP, Colwell R, Bouma MJ (2000) Cholera dynamics and El Niño-Southern Oscillation. *Science* 289:1766–1769.
9. Patz JA, Campbell-Lendrum D, Holloway T, Foley JA (2005) Impact of regional climate change on human health. *Nature* 438:310–317.
10. Rasmusson EM, Wallace JM (1983) Meteorological aspects of the el nino/southern oscillation. *Science* 222:1195–1202.
11. Ropelewski CF, Halpert MS (1987) Global and Regional Scale Precipitation Patterns Associated with the El Niño/Southern Oscillation. *Mon Weather Rev* 115:1606–1626.
12. National Oceanic and Atmospheric Administration (2016) Climate Prediction Center: ENSO diagnostic discussion. Available at www.cpc.ncep.noaa.gov/products/analysis_monitoring/enso_advisory/ensodisc.html. Accessed April 6, 2016.
13. Bellew HW (1885) *The History of Cholera in India from 1862-1881: Being a Descriptive and Statistical Account of the Disease as Derived from the Published Official Reports of the Several Provincial Governments During that Period and Mainly in Illustration of the Relation Between Cholera Activity and Climatic Conditions Together with Original Observations on the Causes and Nature of Cholera* (Trubner & Co., London).
14. Colwell RR (1996) Global climate and infectious disease: The cholera paradigm. *Science* 274:2025–2031.
15. Colwell RR, Huq A (1998) Global microbial ecology: Biogeography and diversity of Vibrios as a model. *J Appl Microbiol* 85:134S–137S.
16. Koelle K, Rodó X, Pascual M, Yunus M, Mostafa G (2005) Refractory periods and climate forcing in cholera dynamics. *Nature* 436:696–700.
17. Rebaudet S, Sudre B, Faucher B, Piarroux R (2013) Environmental determinants of cholera outbreaks in inland Africa: A systematic review of main transmission foci and propagation routes. *J Infect Dis* 208:S46–S54.
18. Bompangue Nkoko D, et al. (2011) Dynamics of cholera outbreaks in Great Lakes region of Africa, 1978-2008. *Emerg Infect Dis* 17:2026–2034.
19. Olago D, et al. (2007) Climatic, socio-economic, and health factors affecting human vulnerability to cholera in the Lake Victoria basin, East Africa. *Ambio* 36:350–358.
20. Umoh JU, Adesiyun AA, Adekeye JO, Nadarajah M (1983) Epidemiological features of an outbreak of gastroenteritis/cholera in Katsina, Northern Nigeria. *J Hyg (Lond)* 91:101–111.
21. Tauxe RV, Holmberg SD, Dodin A, Wells JV, Blake PA (1988) Epidemic cholera in Mali: High mortality and multiple routes of transmission in a famine area. *Epidemiol Infect* 100:279–289.
22. Griffith DC, Kelly-Hope LA, Miller MA (2006) Review of reported cholera outbreaks worldwide, 1995-2005. *Am J Trop Med Hyg* 75:973–977.
23. World Health Organization (2014) Weekly epidemiological record: Cholera articles. Available at www.who.int/cholera/statistics/en. Accessed March 30, 2016.
24. Ali M, Nelson AR, Lopez AL, Sack DA (2015) Updated global burden of cholera in endemic countries. *PLoS Negl Trop Dis* 9:e0003832.
25. Cai W, et al. (2014) Increasing frequency of extreme El Niño events due to greenhouse warming. *Nat Clim Chang* 4:111–116.
26. Latif M, Semenov VA, Park W (2015) Super El Niños in response to global warming in a climate model. *Clim Change* 132:489–500.
27. Santoso A, et al. (2013) Late-twentieth-century emergence of the El Niño propagation asymmetry and future projections. *Nature* 504:126–130.
28. Wang C, Deser C, Yu J-Y, DiNezio P, Clement A (2017) Coral reefs of the eastern tropical Pacific. *El Niño and Southern Oscillation (ENSO): A Review. Coral Reefs of the Eastern Tropical Pacific*, eds Glynn PW, Manzello DP, Enochs IC (Springer, Dordrecht, The Netherlands), pp 85–106.
29. Williams AP, et al. (2011) Recent summer precipitation trends in the Greater Horn of Africa and the emerging role of Indian Ocean sea surface temperature. *Clim Dyn* 39:2307–2328.
30. Tierney JE, Ummenhofer CC, deMenocal PB (2015) Past and future rainfall in the Horn of Africa. *Sci Adv* 1:e1500682.
31. Ludescher J, et al. (2014) Very early warning of next El Niño. *Proc Natl Acad Sci USA* 111:2064–2066.
32. Barnston AG, Tippett MK, L'Heureux ML, Shuhua L, DeWitt DG (2012) Skill of real-time seasonal ENSO model predictions during 2002–11: Is our capability increasing? *Bull Am Meteorol Soc* 93:631–651.
33. United Nations International Children's Emergency Fund (2016) Cholera outbreaks in Central and West Africa: 2016 regional update - Week 06. Available at https://www.unicef.org/cholera/files/WCA_Cholera_Update_W6.pdf. Accessed April 6, 2016.
34. Bivand R, Rundel C (2014) *rgeos: Interface to Geometry Engine - Open Source (GEOS)*. Available at cran.r-project.org/web/packages/rgeos/index.html Accessed November 16, 2016.
35. Lehner B, Bernhard L, Petra D (2004) Development and validation of a global database of lakes, reservoirs and wetlands. *J Hydrol (Amst)* 296:1–22.
36. Pullan RL, Freeman MC, Gething PW, Brooker SJ (2014) Geographical inequalities in use of improved drinking water supply and sanitation across sub-Saharan Africa: Mapping and spatial analysis of cross-sectional survey data. *PLoS Med* 11:e1001626.
37. Hijmans RJ (2015) *raster: Geographic Data Analysis and Modeling*. Available at https://cran.r-project.org/web/packages/raster/index.html. Accessed November 16, 2016.
38. Funk C, et al. (2015) The climate hazards infrared precipitation with stations–A new environmental record for monitoring extremes. *Sci Data* 2:150066.
39. Rodell M, et al. (2004) The Global Land Data Assimilation System. *Bull Am Meteorol Soc* 85:381–394.
40. Didan K (2015) MOD13C2 MODIS/Terra Vegetation Indices Monthly L3 Global 0.05Deg CMG V006, https://dx.doi.org/10.5067/MODIS/MOD13C2.006.
41. Smith TM, Reynolds RW, Peterson TC, Jay L (2008) Improvements to NOAA's historical merged land–ocean surface temperature analysis (1880–2006). *J Clim* 21:2283–2296.
42. Besag J, Julian B, Jeremy Y, Annie M (1991) Bayesian image restoration, with two applications in spatial statistics. *Ann Inst Stat Math* 43:1–20.
43. Banerjee S, Carlin BP, Gelfand AE (2014) *Hierarchical Modeling and Analysis for Spatial Data* (CRC Press, Boca Raton, FL), 2nd Ed.
44. Stern HS, Cressie N (2000) Posterior predictive model checks for disease mapping models. *Stat Med* 19:2377–2397.
45. White G, Ghosh SK (2009) A stochastic neighborhood conditional autoregressive model for spatial data. *Comput Stat Data Anal* 53:3033–3046.
46. Lee D (2011) A comparison of conditional autoregressive models used in Bayesian disease mapping. *Spat Spatio-Temporal Epidemiol* 2:79–89.
47. Nadaraya EA (1964) On estimating regression. *Theory Probab Appl* 9:141–142.
48. Watson GS (1964) Smooth regression analysis. *Sankhya Ser A* 26:359–372.
49. Nychka D, Furrer R, Sain S (2015) *fields: Tools for Spatial Data*. Available at https://cran.r-project.org/web/packages/fields/index.html. Accessed November 16, 2016.
50. Lehner B, Bernhard L, Günther G (2013) Global river hydrography and network routing: Baseline data and new approaches to study the world's large river systems. *Hydrol Processes* 27:2171–2186.